




Article

Influence of GeO₂ Content on the Spectral and Radiation-Resistant Properties of Yb/Al/Ge Co-Doped Silica Fiber Core Glasses

Yiming Zhu ^{1,2} , Yan Jiao ², Yue Cheng ^{1,2} , Chongyun Shao ^{2,*}, Chunlei Yu ^{2,3,*}, Ye Dai ^{1,*}  and Lili Hu ^{2,3}

- ¹ Department of Physics, Shanghai University, Shanghai 200444, China; zym013579@gmail.com (Y.Z.); chengyue@siom.ac.cn (Y.C.)
- ² Key Laboratory of High Power Laser Materials, Shanghai Institute of Optics and Fine Mechanics, Chinese Academy of Sciences, Shanghai 201800, China; jiaoyan@siom.ac.cn (Y.J.); hulili@siom.ac.cn (L.H.)
- ³ Hangzhou Institute for Advanced Study, University of Chinese Academy of Sciences, Hangzhou 310024, China
- * Correspondence: shaochongyun@foxmail.com (C.S.); sdyclly@163.com (C.Y.); yedai@shu.edu.cn (Y.D.)

Abstract: In this study, Yb/Al/Ge co-doped silica fiber core glasses with different GeO₂ contents (0–6.03 mol%) were prepared using the sol–gel method combined with high-temperature sintering. The absorption, fluorescence, radiation-induced absorption, continuous-wave electron paramagnetic resonance spectra, and fluorescence decay curves were recorded and analyzed systematically before and after X-ray irradiation. The effects of GeO₂ content on the valence variations of Yb³⁺/Yb²⁺ ions, spectral properties of Yb³⁺ ions, and radiation resistance of Yb/Al/Ge co-doped silica glasses were systematically studied. The results show that even if the GeO₂ content of the sample is relatively low (0.62 mol%), it can inhibit the generation of Yb²⁺ ions with slight improvement in the spectral properties of Yb³⁺ ions in the pristine samples and effectively improve its radiation resistance. Direct evidence confirms that the generation of trapped-electron centers (Yb²⁺/Si-E'/Al-E') and trapped-hole centers (Al-OHC) was effectively inhibited by Ge co-doping. This study provides a theoretical reference for the development of high-performance, radiation-resistant Yb-doped silica fibers.

Keywords: Yb-doped silica glass; radiation resistance; anti-darkening; color center



Citation: Zhu, Y.; Jiao, Y.; Cheng, Y.; Shao, C.; Yu, C.; Dai, Y.; Hu, L. Influence of GeO₂ Content on the Spectral and Radiation-Resistant Properties of Yb/Al/Ge Co-Doped Silica Fiber Core Glasses. *Materials* **2022**, *15*, 2235. <https://doi.org/10.3390/ma15062235>

Academic Editors: Gianluca Malavasi and Edgar Dutra Zanotto

Received: 12 January 2022

Accepted: 15 March 2022

Published: 17 March 2022

Publisher's Note: MDPI stays neutral with regard to jurisdictional claims in published maps and institutional affiliations.



Copyright: © 2022 by the authors. Licensee MDPI, Basel, Switzerland. This article is an open access article distributed under the terms and conditions of the Creative Commons Attribution (CC BY) license (<https://creativecommons.org/licenses/by/4.0/>).

1. Introduction

Over the past few decades, rare-earth (RE)-doped silica fiber lasers and amplifiers have been studied extensively [1–3]. Owing to their reduced weight, small size, high output power, good beam quality, and high electro-optical conversion efficiency, Yb-doped fiber (YDF) lasers and amplifiers have applications in industrial manufacturing [4], laser lidar [5], space debris removal, and free-space optical communication [6]. However, the high laser output is strictly limited by the fact that YDF suffers from two-fold degradation [7,8], commonly referred to as the photodarkening (PD) and radiation darkening (RD) effects [9,10], when operating in amplifying conditions and harsh environments. PD and RD can be induced by pumping and external ionizing radiation, resulting in additional optical loss and a sharp decline in laser output power and slope efficiency.

Researchers generally conclude that the generation of color centers in the fiber is the main reason for the appearance of the darkening effect. Similar loss variations appear after long-term pumping or γ -ray irradiation, indicating that the types of color centers generated in PD and RD are the same [11]. Although the origin and mechanism of color centers are controversial, many studies have confirmed that Yb²⁺ ions and oxygen hole center defects are the main causes of PD and RD in YDF [12].

The main methods to suppress the effects of PD and RD are gas loading and core composition optimization. Many researchers have demonstrated that H₂-loading is beneficial for improving the radiation resistance of fibers [13,14], but there are some limitations

as well. For example, H_2 molecules can easily escape, the mechanical strength of the coating may decrease, and H_2 causes additional absorption [15]. Even worse, owing to the reducing environment caused by H_2 , Yb^{3+} ions are easily reduced into Yb^{2+} ions [16]. Core composition optimization is the most fundamental method. Ce co-doping has been used to suppress the formation of aluminum-oxygen hole center (Al-OHC) defects [17,18], and the valence variation of $Ce^{4+} \rightarrow Ce^{3+}$ reduces the generation of Yb^{2+} ions and further improves the radiation resistance. However, this presents the problem that Ce co-doping seriously impacts the spectral properties of Yb^{3+} ions [19]. Jetschke et al. proposed a method to improve the PD resistance by Al/P co-doping [20]. However, it reduces the absorption and emission cross-sections of Yb^{3+} ions, and the radiation resistance of the Yb/Al/P co-doped fiber is relatively weak [21,22]. It has been confirmed that Ge co-doping can reduce the radiation-induced absorption (RIA) caused by Al- and/or P-related defects during irradiation [23,24] and improve the radiation resistance of Er/Al/Ge co-doped glasses and fibers without negatively affecting the spectral properties of Er^{3+} ions [25]. However, the effects of Ge co-doping on the spectral and radiation-resistant properties of Yb-doped silica glasses have not yet been reported.

The absorption band caused by radiation-induced color centers is mainly in the ultraviolet–visible range [12]. Limited by Rayleigh scattering, the absorption of the fiber sample is relatively large in the ultraviolet–visible band; therefore, it is difficult to collect accurate data in the fiber. In addition, continuous-wave electron paramagnetic resonance (CW-EPR) is an effective method for studying paramagnetic color centers. Owing to the small size of the fiber core, it is difficult to obtain powder samples for CW-EPR tests. Therefore, in this work, uniform and large-scale Yb/Al/Ge co-doped silica glasses with different GeO_2 contents were prepared using the sol–gel method combined with high-temperature powder sintering. By analyzing the absorption, fluorescence spectra, and fluorescence decay curves of the glasses, the effects of Ge co-doping on the Yb^{2+} ion suppression and the Yb^{3+} ion spectral properties were studied. By comparing the changes in luminescence intensity and fluorescence lifetime of Yb^{3+} ions before and after irradiation, the effect of Ge co-doping on the radiation resistance of Yb/Al/Ge co-doped glasses was studied, and the related mechanisms were revealed by RIA and CW-EPR spectra.

2. Experimental Details

2.1. Sample Preparation

$0.15Yb_2O_3 - 1.5Al_2O_3 - xGeO_2 - (98.35 - x)SiO_2$ (in mol%, $x = 0, 1, 4, 8, 12$) glasses were prepared using the sol–gel method combined with high-temperature powder sintering [26]. The glasses were labeled GAY0, GAY1, GAY4, GAY8, and GAY12 (referred to as GAY samples) based on the theoretical content of GeO_2 . In addition, Al-doped and Ge-doped silica glasses were prepared using the same method for comparative analysis. The actual compositions of the samples were measured using inductively coupled plasma optical emission spectrometry (ICP-OES; radial-view Thermo iCAP 6300, Thermo Fisher Scientific Inc., Waltham, MA, USA). The theoretical and actual compositions are presented in Table 1. The actual Yb_2O_3 content was close to the theoretical values. Even if part of the GeO_2 volatilized, 50–62% of the theoretical content remained. The actual Al content was higher than the theoretical content because the glasses were polluted by the corundum crucible. The samples were polished into bulk glasses of approximately 10 mm diameter and 2 mm thickness for further testing. The powdered samples, which were utilized for the CW-EPR tests, had masses of approximately 100 mg.

Table 1. Theoretical and actual compositions of the GAY, Al-doped, and Ge-doped samples.

Samples	Theoretical Composition (in mol%)			Actual Composition (in mol%)		
	GeO ₂	Yb ₂ O ₃	Al ₂ O ₃	GeO ₂	Yb ₂ O ₃	Al ₂ O ₃
1.5Al	0	0	1.5	0	0	2.11
2Ge	2	0	0	1.17	0	0
GAY0	0	0.15	1.5	0	0.16	2.01
GAY1	1	0.15	1.5	0.62	0.16	2.45
GAY4	4	0.15	1.5	2.36	0.16	2.10
GAY8	8	0.15	1.5	4.12	0.15	2.21
GAY12	12	0.15	1.5	6.03	0.16	2.33

2.2. Analyses of Samples

The densities of the samples were measured using an SD-200L electronic densimeter based on the Archimedes drainage method. The refractive indices of the samples were measured using a 2010/M prism coupler (Metricon Corp., Pennington, NJ, USA). The absorption spectra were measured using a Perkin-Elmer Lambda 950UV/VIS/NIR spectrophotometer. Fluorescence spectra and fluorescence decay curves were measured using an FLS920 steady/transient state high-resolution fluorescence spectrometer (Edinburgh Instruments Ltd., Kirkton Campus, UK). The fluorescence spectra of Yb³⁺ ions were measured using a xenon lamp under 896 nm excitation. The fluorescence decay curves of Yb³⁺ ions were measured at 1020 nm under excitation by a 980 nm LD. The fluorescence spectra and fluorescence decay curves of Yb²⁺ ions were both measured at 525 nm under the excitation of a 330 nm xenon lamp, and the fluorescence decay curve of the Ge oxygen deficiency center (Ge-ODC) was measured at 395 nm under the excitation of a 330 nm xenon lamp.

To study the effect of GeO₂ content on the radiation resistance of Yb/Al/Ge co-doped silica glasses, an X-ray instrument (XRad160, Precision X-Ray, Inc., Madison, WI, USA) was used to irradiate the samples. The total dose and dose rate of irradiation were 3000 Gy and 1440 Gy/h, respectively.

The paramagnetic defects induced by irradiation were recorded using an E-580 Bruker Elexsys X-band EPR spectrometer (Bruker Co., Billerica, MA, USA). The microwave frequency was approximately 9.38 GHz. All the measurements were conducted at room temperature (300 K).

3. Results and Discussion

3.1. Effects of GeO₂ Content on the Spectral Properties of Yb/Al/Ge Co-Doped Silica Glasses

Figure 1a,b show the density and refractive index of the GAY samples with different GeO₂ contents. With an increase in GeO₂ content, the density and refractive index of the samples increased almost linearly. Linear fitting reveals that the slopes of the density and refractive index are approximately $2.26 \times 10^{-2} \text{ g}\cdot\text{cm}^{-3}\cdot\text{mol}^{-1}$ and $1.85 \times 10^{-5} \text{ mol}^{-1}$. Although Ge co-doping may cause a higher refractive index of the fiber core, the numerical aperture (NA) of the fiber can still be controlled by creating a graded refractive index layer [27,28].

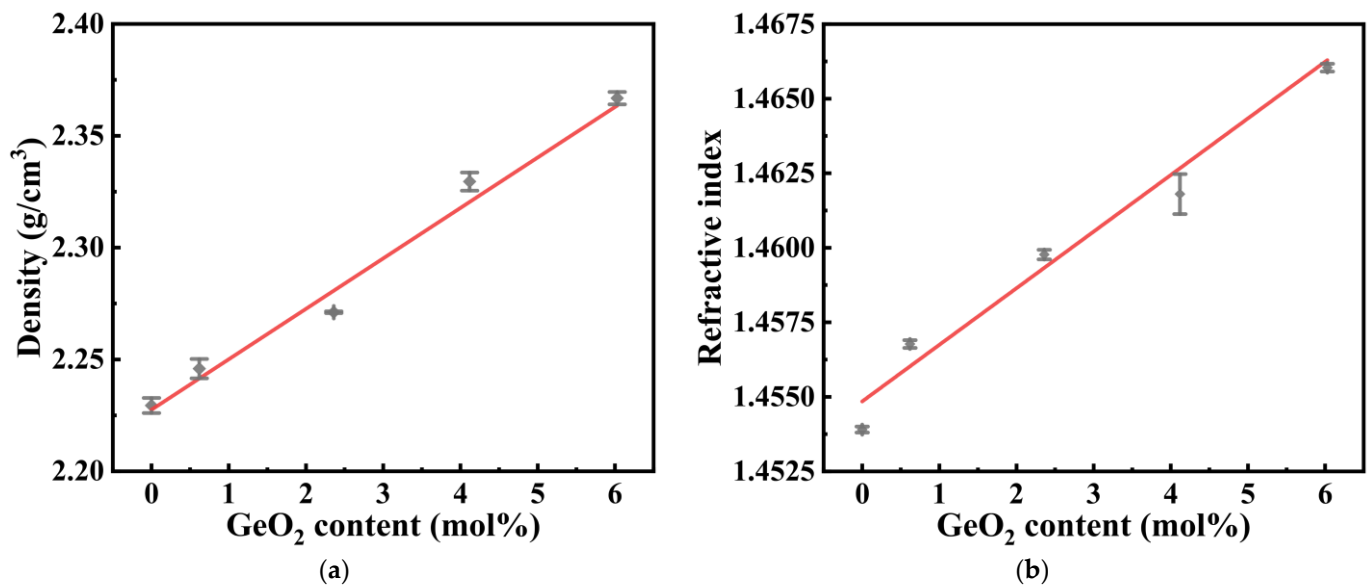


Figure 1. (a) Density and (b) refractive index of GAY samples.

Figure 2a shows the absorption spectra of the pristine GAY samples with different GeO₂ contents in the range of 270–550 nm. The Ge-free (GAY0) sample has an absorption band at 330–450 nm, which is primarily attributed to the 4f–5d transition of Yb²⁺ ions [29,30]. With an increase in the GeO₂ content, the absorption intensity of the Yb²⁺ ions is significantly reduced. Even in the GAY1 sample (GeO₂ content of 0.62 mol%), the absorption intensity of Yb²⁺ ions is very weak. This shows that a low doping concentration of Ge can effectively suppress the formation of Yb²⁺ ions. As shown in the inset of Figure 2a, owing to the higher absorption intensity of Yb²⁺ ions, the GAY0 sample was yellowish. In contrast, the GAY12 sample was colorless and transparent.

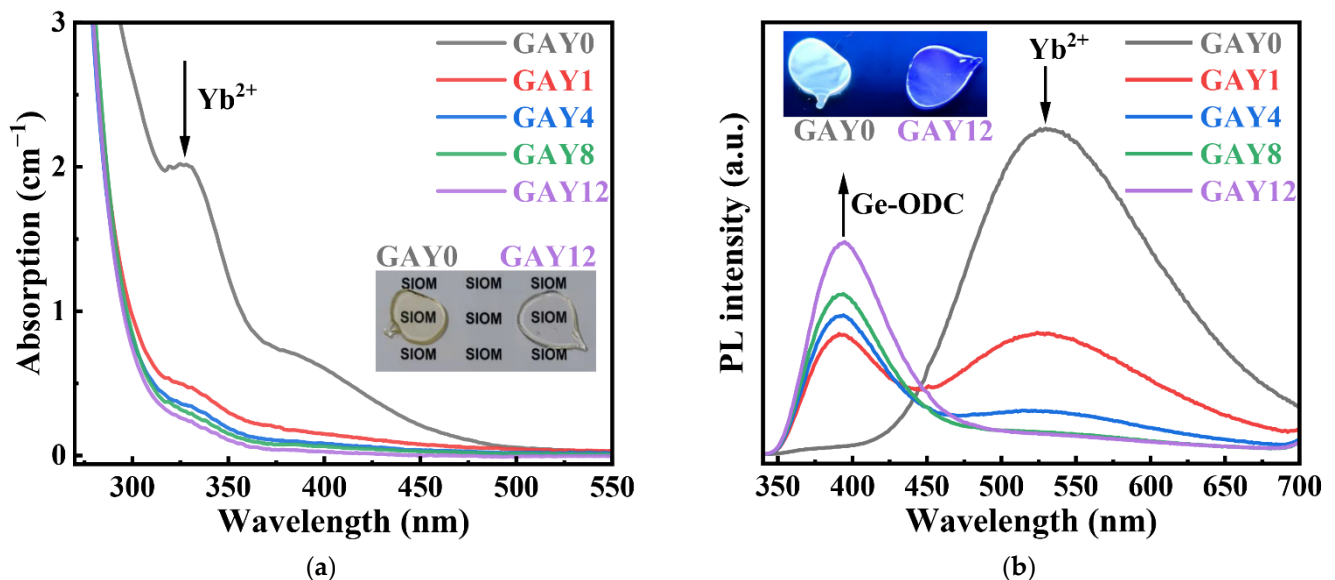


Figure 2. (a) Absorption and (b) fluorescence of pristine GAY samples; comparison photographs of GAY0 and GAY12 samples (inset in (a)) under natural light and (inset in (b)) under ultraviolet light.

Figure 2b shows the fluorescence spectra of the pristine GAY samples in the range of 340–700 nm excited by a 330 nm xenon lamp. The fluorescence spectrum of the GAY0 sample has a very broad emission band at 525 nm, which was caused by Yb²⁺ ion emission [29], and it is primarily attributed to the 4f–5d transition of Yb²⁺ ions [30]. With an increase in

the GeO₂ content, the fluorescence intensity of Yb²⁺ ions decreased, and a new fluorescence peak appeared and increased simultaneously at 395 nm, which can be attributed to the Ge-ODC defect emission [31]. The absorption of Ge-ODC mainly originates from the S₀→S₁ transition, and the emission of Ge-ODC primarily originates from the transition of T₁→S₀. The energy level diagram of Ge-ODC can be found in Ref. [32]. As shown in the inset of Figure 2b, the GAY0 sample emits yellowish light under ultraviolet light, which is mainly attributed to the emission of Yb²⁺ ions. Meanwhile, mainly attributed to the emission of Ge-ODC defects, the GAY12 sample emits bluish light. These results further confirm that Ge co-doping can effectively suppress the generation of Yb²⁺ ions.

Figure 3 shows the fluorescence decay curves of Yb²⁺ ions and Ge-ODC. The lifetime of Yb²⁺ ions measured at 525 nm under 330 nm excitation with the GAY0 sample is 58.1 μs [33]. The lifetime of Ge-ODC measured at 395 nm under 330 nm excitation with a high GeO₂ content (GAY12) sample is 95.1 μs. The results confirm that the fluorescence peaks at 525 nm and 395 nm (see Figure 2b) originate from two different fluorescence centers of Yb²⁺ and Ge-ODC, respectively.

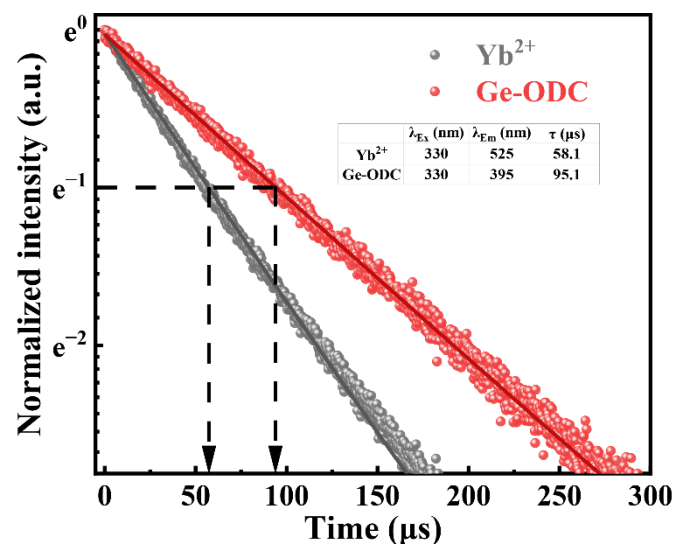


Figure 3. Fluorescence decay curves of Yb²⁺ ions and Ge-ODC.

Figure 4a,b show the absorption and fluorescence spectra of Yb³⁺ ions in the GAY samples. The absorption and emission of Yb³⁺ primarily originates from 4f–5d transition [30]. The absorption curves of the samples with different GeO₂ contents roughly overlap, and the absorption intensities of the samples at 976 nm are almost the same. In addition, the fluorescence spectra of the samples under 896 nm excitation roughly coincide. The fluorescence intensity of the Ge co-doped samples is slightly higher than that of GAY0. This may be due to the suppression of Ge co-doping with Yb²⁺ ions. This proves that Ge co-doping has no negative impact on the absorption and fluorescence spectra of Yb³⁺ ions.

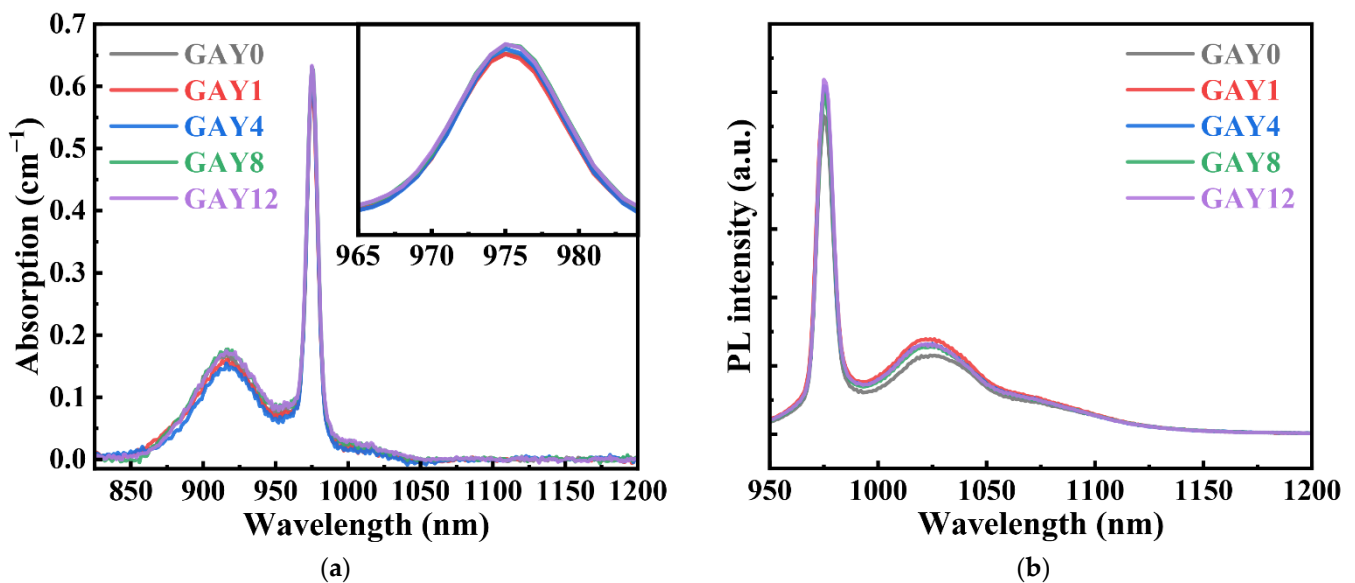


Figure 4. (a) Absorption spectra, (inset: enlargement in the range of 965–984 nm), (b) Fluorescence spectra of pristine GAY samples.

Figure 5 shows the absorption cross-section at 976 nm, emission cross-section, and fluorescence lifetime at 1020 nm of Yb^{3+} ions. The absorption and emission cross-sections were calculated using the Lambert–Beer law and the Fuchtbauer–Lademurg (F–L) formula [34]. With an increase in the GeO_2 content, the absorption cross-section and emission cross-section of Yb^{3+} ions hardly changed, but the fluorescence lifetime of Yb^{3+} ions increased gradually.

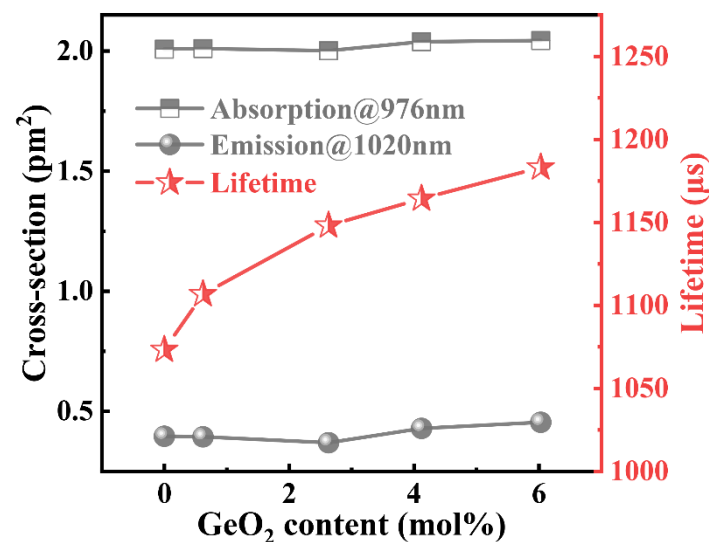
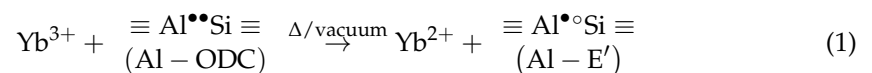


Figure 5. Absorption, emission cross-section, and fluorescence lifetime of Yb^{3+} ions in pristine GAY samples.

The formation mechanism of Yb^{2+} ions in Yb/Al co-doped silica glasses during vacuum sintering may be related to the disappearance of Al-related oxygen deficiency centers (Al-ODC). The corresponding chemical reactions are as follows:



where, “•” and “°” represent an electron and a hole, respectively. This speculation is supported by the results of Kirchhof et al. [30]. Al-, P-, and Ge-related oxygen defect centers (ODC) are easily formed during sintering in a vacuum or inert atmosphere (e.g., He). However, Kirchhof et al. found that in 6P₂O₅-94SiO₂ and 7GeO₂-93SiO₂ (in mol%) glasses sintered in an inert atmosphere, the introduction of Yb³⁺ ions did not significantly change the fluorescence intensity of Ge-ODC and P-ODC, and no Yb²⁺ ion fluorescence was detected. In contrast, in 4Al₂O₃-0.5P₂O₅-95.5SiO₂ (in mol%) glasses sintered in an inert atmosphere, the introduction of Yb³⁺ ions significantly reduced the fluorescence intensity of Al-ODC, and meanwhile, the fluorescence of Yb²⁺ ions was detected. Herein, with an increase in the GeO₂ content, Ge-ODC became the main ODC defect at the expense of Al-ODC. Therefore, Yb²⁺ ions were gradually inhibited.

3.2. Effects of GeO₂ Content on the Radiation Resistance of Yb/Al/Ge Co-Doped Silica Glasses

Figure 6a,b show the fluorescence integral intensity in the range of 950–1200 nm and fluorescence lifetime at 1020 nm of the GAY samples before and after irradiation. Before irradiation, with an increase in the GeO₂ content, both the fluorescence integral intensity and fluorescence lifetime of Yb³⁺ ions increased slightly. The increase in the fluorescence integral intensity may be related to the oxidation of Yb²⁺ ions to Yb³⁺ ions. The increase in the fluorescence lifetime may be related to the low phonon energy caused by the coordination of Ge to Yb³⁺ ions. After irradiation, the fluorescence integral intensity and fluorescence lifetime of all samples decreased. The fluorescence integral intensity and fluorescence lifetime of the GAY0 sample showed the largest decrease. Meanwhile, with increasing GeO₂ content, the difference decreased. This result shows that Ge co-doping can effectively improve the radiation resistance of Yb/Al co-doped silica glasses.

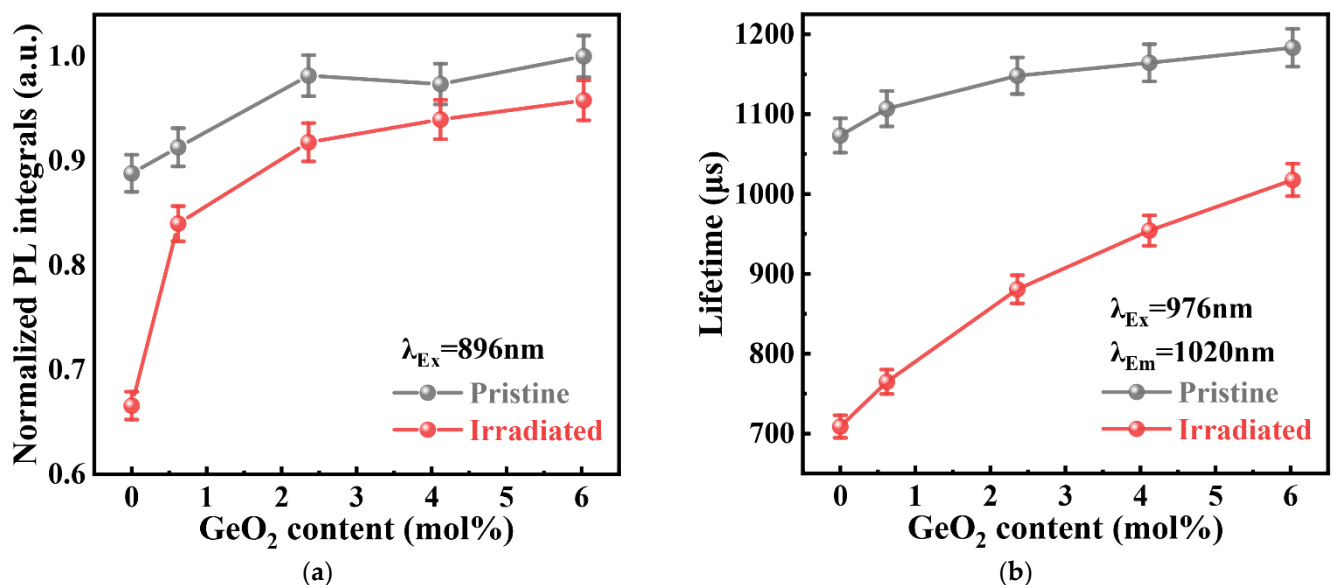


Figure 6. (a) Fluorescence integral intensity and (b) fluorescence lifetime of GAY samples before and after irradiation.

Previous studies have shown that the darkening effect of YDF is related to the valence variations of Yb^{2+/3+} ions and the formation of dopant-related point defects [16,21]. Compared with Yb²⁺ ions, point defects have a larger absorption cross-section and wider absorption band, and they are closer to the absorption and emission wavelengths of Yb³⁺ ions; therefore, they significantly impact the spectral properties of Yb³⁺ ions.

The Al-doped and Ge-doped silica glasses without Yb³⁺ ions were prepared to eliminate the contribution of Yb²⁺ ion absorption to the RIA (see Figure 7a,b). The cumulative fitted peaks were consistent with the observed RIA. The RIA spectrum of the Al-doped sample was decomposed into six Gaussian components with peaks at 2.2, 2.9, 4.2, 4.8, 5.1, and 5.8 eV.

These bands can be attributed to the Al-OHC defect ($\equiv\text{Al-O}^\circ$, 2.2 and 2.9 eV) [35], aluminum dangling bond (Al-E') defect (4.2 eV) [35], peroxy radical (POR) defect (4.8 eV) [35], Al-ODC defect (5.1 eV), and silicon dangling bond (Si-E') defect (5.8 eV) [36]. The RIA spectrum of the Ge-doped sample was decomposed into five Gaussian components with peaks at 4.6, 5.1, 5.6, 5.8, and 6.4 eV. These bands can be attributed to the Ge(1) defect (4.6 eV) [37], Ge-ODC (5.1 eV) [38], Ge(2) defect (5.6 eV) [39], Si-E' defect (5.8 eV) [36], and germanium dangling bond (Ge-E') defect (6.4 eV) [40]. The RIA intensity of the Ge-ODC defects was negative, which means that the content of Ge-ODC decreased after irradiation. The RIA intensities of the other defect centers were all positive, which means that the contents of these defects increased after irradiation.

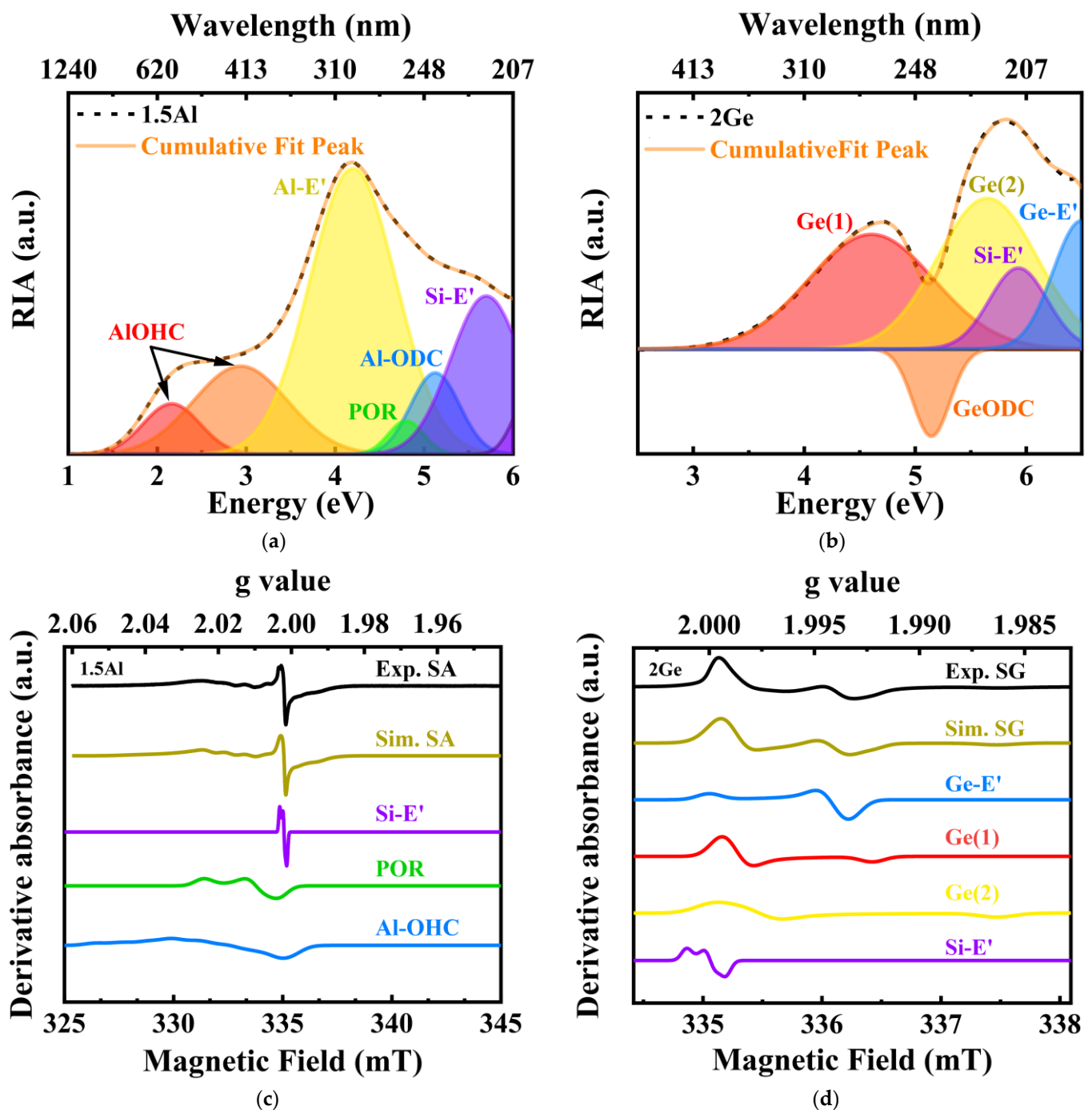


Figure 7. Gaussian decomposition of RIA of (a) Al-doped and (b) Ge-doped glasses; CW-EPR spectra of irradiated (c) Al-doped and (d) Ge-doped glasses.

Figure 7c,d show the CW-EPR spectra of the Al-doped and Ge-doped silica glasses after irradiation. The CW-EPR spectrum of the Al-doped sample was decomposed into three parts, corresponding to the POR, Si-E', and Al-OHC defect centers. Theoretically, owing to the hyperfine coupling interaction between the holes and the magnetic core ^{27}Al ($I = 5/2$, $NA \sim 100\%$), six hyperfine lines can be observed at each g component ($g_1, g_2, g_3, 2I + 1 = 6$). However, since the hyperfine lines of the g components are superimposed on each other, this phenomenon is difficult to observe experimentally. The CW-EPR spectrum of the Ge-doped samples was decomposed into four parts, corresponding to the Ge-E', Ge(1), Ge(2), and Si-E' defect centers. Since the natural abundance of the magnetic core ^{73}Ge is only 7.76%, no hyperfine lines for the Ge-E', Ge(1), or Ge(2) defects are observed in this EPR spectrum.

Al-ODC and Ge-ODC are diamagnetic centers (no CW-EPR signal) and cannot be detected in the CW-EPR test. Although the Al-E' defect is a paramagnetic center, since its spin-lattice relaxation time is relatively long, it is usually detectable only in the scattering (non-absorption) mode and very low microwave power [36]. Therefore, the CW-EPR signal of the Al-E' defect cannot be observed in Figure 7c.

Figure 8a,b show the RIA and CW-EPR spectra of the GAY samples. In contrast to the fitting results in Figure 7, the absorption of the RIA at 540 nm in Figure 8a is mainly attributed to Al-OHC, and the RIA in the ultraviolet band is mainly attributed to Ge-related defects. In Figure 8b, the signal of CW-EPR at 331 mT is also mainly attributed to Al-OHC defects, and the CW-EPR signal in the central region (334–337 mT) is mainly attributed to Ge-related defects. Figure 8a,b show that with an increase in the GeO_2 content, the RIA and CW-EPR intensity of the Al-OHC decreased significantly, and the RIA and CW-EPR intensity of the Ge-related defects gradually increased. Compared with Ge-related defects, the absorption band of Al-OHC defects is closer to the infrared band, and the extension of its absorption band can even cover 1 μm . Therefore, compared to Al-OHC, Ge-related defects have a slighter impact on the spectral properties of Yb^{3+} ions.

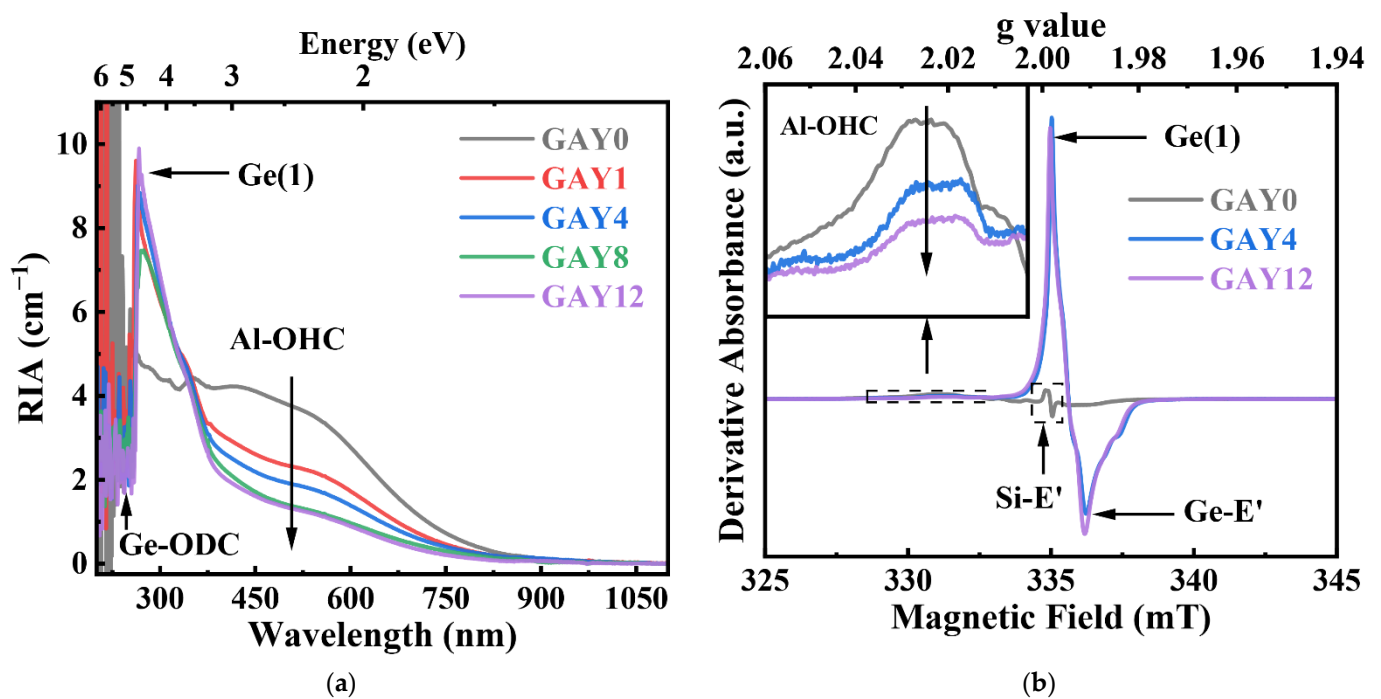
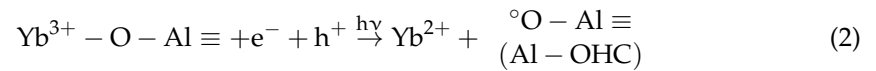
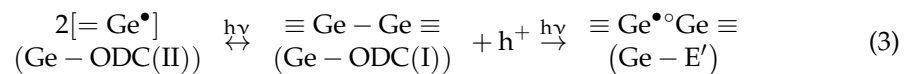


Figure 8. (a) RIA and (b) CW-EPR spectra of irradiated GAY samples.

Previous studies have shown that in Yb/Al co-doped silica glasses, Yb³⁺ ions are coordinated in [AlO_{4/2}][−] tetrahedra, and the following reactions occur during the irradiation process [21,25]:



In Yb/Al/Ge co-doped silica glasses, the content of Ge-ODC increases with increasing GeO₂ content. There are two types of Ge-ODC color centers (Ge-ODC(I) and Ge-ODC(II)), which can be converted into each other during the irradiation process. The presence of Ge-ODC was confirmed by the fluorescence spectra (see Figure 2b). Since Ge-ODC(I) has a stronger ability to capture holes than the [AlO_{4/2}][−] group [41], Ge co-doping enables Ge-ODC(I) to capture more holes, thereby increasing the radiation-induced Ge-E' content, as follows:



Meanwhile, the number of holes captured by the [AlO_{4/2}][−] group is reduced, thereby reducing the Al-OHC content. Figure 8a shows a cavity that appears in the RIA curve at 248 nm, which indicates that the Ge-ODC content decreases after irradiation. With an increase in the GeO₂ content, the intensity of the RIA curve weakens at 540 nm, which means that the Al-OHC defect content decreases. In addition, as the number of [GeO_{4/2}]⁰ groups increases with increasing GeO₂ content, additional electrons are captured by the [GeO_{4/2}]⁰ groups to form Ge(1) and Ge(2) color centers, and the formula is as follows:

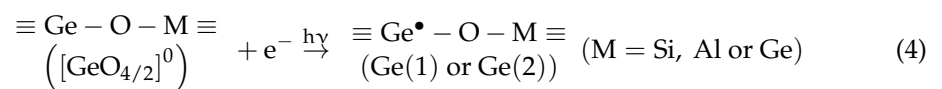


Figure 8a shows that the intensity of the RIA curve increases significantly with an increase in the GeO₂ content at 269 nm, which indicates an increase in the Ge(1) defect content. Figure 8b shows that the CW-EPR intensity of Ge(1) and Ge-E' defects increases with increasing GeO₂ content. This process suppresses the formation of other trapped-electron centers (Yb²⁺/Si-E'/Al-E').

4. Conclusions

Herein, the effects of Ge co-doping on the valence state of Yb^{2+/3+} ions, spectral properties of Yb³⁺ ions, and radiation resistance of Yb/Al/Ge co-doped silica glasses were studied systematically. For the pristine GAY samples, with an increase in the GeO₂ content, the generation of Yb²⁺ ions was considerably suppressed, and the spectral properties of Yb³⁺ ions were improved slightly. After X-ray irradiation, the RIA and CW-EPR spectra confirmed that the Al-OHC defects were effectively inhibited by Ge co-doping. In addition, the fluorescence integral intensity and fluorescence lifetime results also confirmed that the radiation resistance of the samples was improved with increasing GeO₂ content.

The generation and suppression mechanism of Yb²⁺ ions in the pristine Yb/Al/Ge co-doped silica glasses and color centers in irradiated samples are discussed. For the pristine samples, Al-ODC trapped holes to form Al-E' defects during high-temperature sintering. With increasing GeO₂ content, Ge-ODC became the main ODC defect at the expense of Al-ODC. Thus, the relatively stable Ge-ODC inhibited the process by which Yb³⁺ ions trap electrons to form Yb²⁺ ions. When the Yb/Al/Ge co-doped silica glasses were irradiated, the [AlO_{4/2}][−] groups trapped holes to form Al-OHC, and Yb³⁺ ions trapped electrons to form Yb²⁺ ions. Since Ge-ODC has a stronger ability to capture holes than [AlO_{4/2}][−] groups, the formation of trapped-hole centers (Al-OHC) was inhibited. With an increase in the GeO₂ content, the increasing [GeO_{4/2}]⁰ groups formed Ge(1) and Ge(2) color centers by trapping electrons. This process inhibited the formation of all other types of

trapped-electron centers ($\text{Yb}^{2+}/\text{Si-E}'/\text{Al-E}'$). This work suggests that Ge co-doping can be effective for suppressing the generation of Yb^{2+} ions and improving the radiation resistance of Yb-doped silica glasses.

Author Contributions: Y.Z. and Y.J. contributed equally to this work. Conceptualization, C.S., C.Y. and Y.D.; methodology, Y.Z. and Y.J.; validation, Y.Z. and Y.J.; formal analysis, Y.Z., Y.J., C.S., C.Y. and Y.D.; investigation, Y.Z. and Y.C.; resources, Y.J. and C.Y.; data curation, Y.Z. and Y.J.; writing—original draft preparation, Y.Z.; writing—review and editing, Y.J., C.S., C.Y. and Y.C.; funding acquisition, C.Y., C.S. and L.H. All authors have read and agreed to the published version of the manuscript.

Funding: This research was funded by the National Natural Science Foundation of China (NSFC) (Grant Nos. 62005297, 61875216, and 61775224) and the Shanghai Sailing Program (Grant No. 20YF1455300).

Institutional Review Board Statement: Not applicable.

Informed Consent Statement: Not applicable.

Data Availability Statement: The data that support the findings of this study are contained within the article.

Conflicts of Interest: The authors declare no conflict of interest.

References

1. Pask, H.M.; Carman, R.J.; Hanna, D.C.; Tropper, A.C.; Mackechnie, C.J.; Barber, P.R.; Dawes, J.M. Ytterbium-Doped Silica Fiber Lasers: Versatile Sources for the 1–1.2 μm Region. *IEEE J. Sel. Top. Quantum Electron.* **1995**, *1*, 2–13. [[CrossRef](#)]
2. Zhang, Z.X.; Tian, J.R.; Xu, C.X.; Xu, R.Q.; Cui, Y.S.; Zhuang, B.H.; Song, Y.R. Noise-like pulse with a 690 fs pedestal generated from a nonlinear Yb-doped fiber amplification system. *Chin. Opt. Lett.* **2020**, *18*, 5. [[CrossRef](#)]
3. Ye, Y.; Lin, X.F.; Xi, X.M.; Shi, C.; Yang, B.L.; Zhang, H.W.; Wang, X.L.; Li, J.Y.; Xu, X.J. Novel constant-cladding tapered-core ytterbium-doped fiber for high-power fiber laser oscillator. *High Power Laser Sci. Eng.* **2021**, *9*, 7. [[CrossRef](#)]
4. Avilov, V.; Fritzsche, A.; Bachmann, M.; Gumenyuk, A.; Rethmeier, M. Full penetration laser beam welding of thick duplex steel plates with electromagnetic weld pool support. *J. Laser Appl.* **2016**, *28*, 7. [[CrossRef](#)]
5. Carlson, C.G.; Dragic, P.D.; Graf, B.W.; Price, R.K.; Coleman, J.J.; Swenson, G.R. High power Yb-doped fiber laser-based LIDAR for space weather. In Proceedings of the Conference on Fiber Lasers V, San Jose, CA, USA, 21–24 January 2008.
6. Wright, M.W.; Valley, G.C. Yb-doped fiber amplifier for deep-space optical communications. *J. Lightwave Technol.* **2005**, *23*, 1369–1374. [[CrossRef](#)]
7. Paschotta, R.; Nilsson, J.; Barber, P.R.; Caplen, J.E.; Tropper, A.C.; Hanna, D.C. Lifetime quenching in Yb-doped fibres. *Opt. Commun.* **1997**, *136*, 375–378. [[CrossRef](#)]
8. She, S.F.; Liu, B.; Chang, C.; Xu, Y.T.; Xiao, X.S.; Cui, X.X.; Li, Z.; Zheng, J.K.; Gao, S.; Zhang, Y.; et al. Yb/Ce Codoped Aluminosilicate Fiber With High Laser Stability for Multi-kW Level Laser. *J. Lightwave Technol.* **2020**, *38*, 6924–6931. [[CrossRef](#)]
9. Koponen, J.J.; Soderlund, M.J.; Hoffman, H.J.; Tammela, S.K.T. Measuring photodarkening from single-mode ytterbium doped silica fibers. *Opt. Express* **2006**, *14*, 11539–11544. [[CrossRef](#)]
10. Dardaillon, R.; Lancry, M.; Myara, M.; Palermo, C.; Signoret, P. Radiation-induced absorption and photobleaching in erbium Al-Ge-codoped optical fiber. *J. Mater. Sci.* **2020**, *55*, 14326–14335. [[CrossRef](#)]
11. Engholm, M.; Norin, L. Preventing photodarkening in ytterbium-doped high power fiber lasers; correlation to the UV-transparency of the core glass. *Opt. Express* **2008**, *16*, 1260–1268. [[CrossRef](#)]
12. Arai, T.; Ichii, K.; Tanigawa, S.; Fujimaki, M. Gamma-radiation-induced photodarkening in ytterbium-doped silica glasses. In Proceedings of the Conference on Fiber Lasers VIII—Technology, Systems, and Applications, San Francisco, CA, USA, 24–27 January 2011.
13. Zotov, K.V.; Likhachev, M.E.; Tomashuk, A.L.; Bubnov, M.M.; Yashkov, M.V.; Guryanov, A.N. Radiation-resistant erbium-doped silica fibre. *Quantum Electron.* **2007**, *37*, 946–949. [[CrossRef](#)]
14. Cao, R.T.; Chen, G.; Chen, Y.S.; Zhang, Z.L.; Lin, X.F.; Dai, B.; Yang, L.Y.; Li, J.Y. Effective suppression of the photodarkening effect in high-power Yb-doped fiber amplifiers by H_2 loading. *Photonics Res.* **2020**, *8*, 288–295. [[CrossRef](#)]
15. Zotov, K.V.; Likhachev, M.E.; Tomashuk, A.L.; Bubnov, M.M.; Yashkov, M.V.; Guryanov, A.N.; Klyamkin, S.N. Radiation-Resistant Erbium-Doped Fiber for Spacecraft Applications. *IEEE Trans. Nucl. Sci.* **2008**, *55*, 2213–2215. [[CrossRef](#)]
16. Rydberg, S.; Engholm, M. Experimental evidence for the formation of divalent ytterbium in the photodarkening process of Yb-doped fiber lasers. *Opt. Express* **2013**, *21*, 6681–6688. [[CrossRef](#)]
17. Shao, C.Y.; Xu, W.B.; Ollier, N.; Guzik, M.; Boulon, G.; Yu, L.; Zhang, L.; Yu, C.L.; Wang, S.K.; Hu, L.L. Suppression mechanism of radiation-induced darkening by Ce doping in Al/Yb/Ce-doped silica glasses: Evidence from optical spectroscopy, EPR and XPS analyses. *J. Appl. Phys.* **2016**, *120*, 8. [[CrossRef](#)]

18. Liu, R.; Yan, D.P.; Chen, M.; Wang, J.M.; Shi, J.H.; Zhu, Q.X. Fabrication of Yb/Ce/P co-doped fluoroaluminosilicate fiber with excellent photodarkening suppression and kW-level laser performance. *Opt. Mater. Express* **2020**, *10*, 777–786. [[CrossRef](#)]
19. Sheng, Y.B.; Yang, L.Y.; Luan, H.X.; Liu, Z.J.; Yu, Y.; Li, J.Y.; Dai, N.L. Improvement of radiation resistance by introducing CeO₂ in Yb-doped silicate glasses. *J. Nucl. Mater.* **2012**, *427*, 58–61. [[CrossRef](#)]
20. Jetschke, S.; Unger, S.; Schwuchow, A.; Leich, M.; Kirchhof, J. Efficient Yb laser fibers with low photodarkening by optimization of the core composition. *Opt. Express* **2008**, *16*, 15540–15545. [[CrossRef](#)]
21. Shao, C.Y.; Ren, J.J.; Wang, F.; Ollier, N.; Xie, F.H.; Zhang, X.Y.; Zhang, L.; Yu, C.L.; Hu, L.L. Origin of Radiation-Induced Darkening in Yb³⁺/Al³⁺/P⁵⁺-Doped Silica Glasses: Effect of the P/Al Ratio. *J. Phys. Chem. B* **2018**, *122*, 2809–2820. [[CrossRef](#)]
22. Shao, C.Y.; Guo, M.T.; Zhang, Y.; Zhou, L.; Guzik, M.; Boulon, G.; Yu, C.L.; Chen, D.P.; Hu, L.L. 193 nm excimer laser-induced color centers in Yb³⁺/Al³⁺/P⁵⁺-doped silica glasses. *J. Non-Cryst. Solids* **2020**, *544*, 8. [[CrossRef](#)]
23. Leon, M.; Lancry, M.; Ollier, N.; Babu, B.H.; Bigot, L.; El Hamzaoui, H.; Savelii, I.; Pastouret, A.; Burov, E.; Trompier, F.; et al. Ge- and Al-related point defects generated by gamma irradiation in nanostructured erbium-doped optical fiber preforms. *J. Mater. Sci.* **2016**, *51*, 10245–10261. [[CrossRef](#)]
24. Kobayashi, Y.; Sekiya, E.H.; Saito, K.; Nishimura, R.; Ichii, K.; Araki, T. Effects of Ge Co-Doping on P-Related Radiation-Induced Absorption in Er/Yb-Doped Optical Fibers for Space Applications. *J. Lightwave Technol.* **2018**, *36*, 2723–2729. [[CrossRef](#)]
25. Jiao, Y.; Yang, Q.B.; Guo, M.T.; Ma, X.B.; Shao, C.Y.; Yu, C.L.; Hu, L.L. Effect of the GeO₂ content on the radiation resistance of Er³⁺-doped silica glasses and fibers. *Opt. Mater. Express* **2021**, *11*, 1885–1897. [[CrossRef](#)]
26. Wang, S.K.; Li, Z.L.; Yu, C.L.; Wang, M.; Feng, S.Y.; Zhou, Q.L.; Chen, D.P.; Hu, L.L. Fabrication and laser behaviors of Yb³⁺ doped silica large mode area photonic crystal fiber prepared by sol–gel method. *Opt. Mater.* **2013**, *35*, 1752–1755. [[CrossRef](#)]
27. Sidharthan, R.; Ji, J.H.; Lim, K.J.; Lim, S.H.; Li, H.Z.; Lua, J.W.; Zhou, Y.N.; Tse, C.H.; Ho, D.; Seng, Y.M.; et al. Step-index high-absorption Yb-doped large-mode-area fiber with Ge-doped raised cladding. *Opt. Lett.* **2018**, *43*, 5897–5900. [[CrossRef](#)]
28. Lim, K.J.; Seah, S.K.W.; Ye, J.Y.; Lim, W.W.; Seah, C.P.; Tan, Y.B.; Tan, S.T.; Lim, H.T.; Sidharthan, R.; Prasad, A.R.; et al. High absorption large-mode area step-index fiber for tandem-pumped high-brightness high-power lasers. *Photonics Res.* **2020**, *8*, 1599–1604. [[CrossRef](#)]
29. Wang, S.; Lou, F.; Yu, C.; Zhou, Q.; Wang, M.; Feng, S.; Chen, D.; Hu, L.; Chen, W.; Guzik, M.; et al. Influence of Al³⁺ and P⁵⁺ ion contents on the valence state of Yb³⁺ ions and the dispersion effect of Al³⁺ and P⁵⁺ ions on Yb³⁺ ions in silica glass. *J. Mater. Chem. C* **2014**, *2*, 4406–4414. [[CrossRef](#)]
30. Kirchhof, J.; Unger, S.; Schwuchow, A.; Jetschke, S.; Reichel, V.; Leich, M.; Scheffel, A. The influence of Yb²⁺ ions on optical properties and power stability of ytterbium doped laser fibers. In Proceedings of the Conference on Optical Components and Materials VII, San Francisco, CA, USA, 26–28 January 2010.
31. Agnello, S.; Boscaino, R.; Cannas, M.; Gelardi, F.M.; La Mattina, F.; Grandi, S.; Magistris, A. Ge related centers induced by gamma irradiation in sol–gel Ge-doped silica. *J. Non-Cryst. Solids* **2003**, *322*, 134–138. [[CrossRef](#)]
32. Kanjilal, A.; Tsushima, S.; Gotz, C.; Rebohle, L.; Voelskow, M.; Skorupa, W.; Helm, M. The role of Ge-related oxygen-deficiency centers in controlling the blue-violet photo- and electroluminescence in Ge-rich SiO₂ via Er doping. *J. Appl. Phys.* **2009**, *106*, 063112. [[CrossRef](#)]
33. Liu, S.; Zheng, S.P.; Tang, C.M.; Li, X.; Xu, W.B.; Sheng, Q.C.; Chen, D.P. Photoluminescence and radioluminescence properties of Yb²⁺-doped silica glass. *Mater. Lett.* **2015**, *144*, 43–45. [[CrossRef](#)]
34. Cheng, Y.; Yang, Q.B.; Yu, C.L.; Guo, M.T.; Jiao, Y.; Dai, Y.; Wang, S.K.; Hu, L.L. Temperature dependence of the spectral properties of Yb³⁺/P⁵⁺/Al³⁺ co-doped silica fiber core glasses. *Opt. Mater. Express* **2021**, *11*, 2459–2467. [[CrossRef](#)]
35. Lagomacini, J.C.; Bravo, D.; Martin, A.; Lopez, F.J.; Martin, P.; Ibarra, A. Growth kinetics of AlOHC defects in γ -irradiated silica glasses. *J. Non-Cryst. Solids* **2014**, *403*, 5–8. [[CrossRef](#)]
36. Hosono, H.; Kawazoe, H. Radiation-induced coloring and paramagnetic centers in synthetic SiO₂:Al glasses. *Nucl. Instrum. Methods Phys. Res. Sect. B-Beam Interact. Mater. Atoms* **1994**, *91*, 395–399. [[CrossRef](#)]
37. Skuja, L. Isoelectronic series of twofold coordinated Si, Ge, and Sn atoms in glassy SiO₂: A luminescence study. *J. Non-Cryst. Solids* **1992**, *149*, 77–95. [[CrossRef](#)]
38. Takahashi, M.; Shigemura, H.; Kawamoto, Y.; Nishii, J.; Yoko, T. Photochemical reactions of Ge-related defects in 10GeO₂·90SiO₂ glass prepared by sol–gel process. *J. Non-Cryst. Solids* **1999**, *259*, 149–155. [[CrossRef](#)]
39. Agnello, S.; Alessi, A.; Gelardi, F.M.; Boscaino, R.; Parlato, A.; Grandi, S.; Magistris, A. Effect of oxygen deficiency on the radiation sensitivity of sol-gel Ge-doped amorphous SiO₂. *Eur. Phys. J. B* **2008**, *61*, 25–31. [[CrossRef](#)]
40. Watanabe, Y.; Kawazoe, H.; Shibuya, K.; Muta, K. Structure and Mechanism of Formation of Drawing- or Radiation-Induced Defects in SiO₂:GeO₂ Optical Fiber. *Jpn. J. Appl. Phys.* **1986**, *25*, 425–431. [[CrossRef](#)]
41. Essid, M.; Albert, J.; Brebner, J.L.; Awazu, K. Correlation between oxygen-deficient center concentration and KrF excimer laser induced defects in thermally annealed Ge-doped optical fiber preforms. *J. Non-Cryst. Solids* **1999**, *246*, 39–45. [[CrossRef](#)]